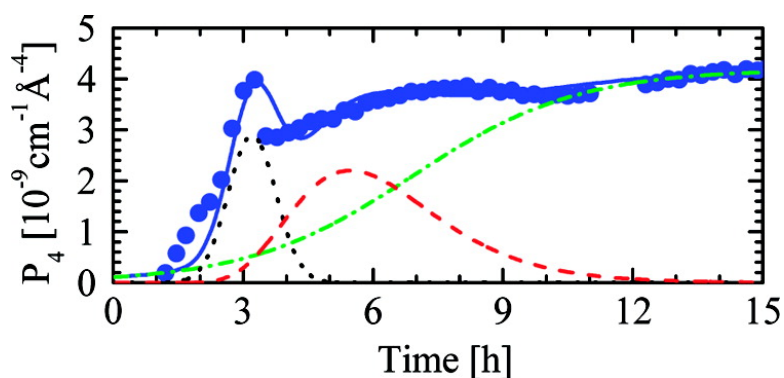Article

Nucleation and Growth of CaCO Mediated by the Egg-White Protein Ovalbumin: A Time-Resolved *in situ* Study Using Small-Angle Neutron Scattering

Vitaliy Pipich, Mathias Balz, Stephan E. Wolf, Wolfgang Tremel, and Dietmar Schwahn

More About This Article

Additional resources and features associated with this article are available within the HTML version:

- Supporting Information
- Links to the 2 articles that cite this article, as of the time of this article download
- Access to high resolution figures
- Links to articles and content related to this article
- Copyright permission to reproduce figures and/or text from this article

View the Full Text HTML

Nucleation and Growth of CaCO₃ Mediated by the Egg-White Protein Ovalbumin: A Time-Resolved *in situ* Study Using Small-Angle Neutron Scattering

Vitaliy Pipich,[†] Mathias Balz,[‡] Stephan E. Wolf,[‡] Wolfgang Tremel,*,[‡] and Dietmar Schwahn*,[†]

Institute of Solid State Research of the Helmholtz Research Center Jülich GmbH, D-52425 Jülich, Germany, and Institute for Inorganic Chemistry, Johannes Gutenberg University, Duesbergweg 10-14, D-55099 Mainz, Germany

Received March 12, 2008; E-mail: d.schwahn@fz-juelich.de; tremel@mail.unimainz.de

Abstract: Mineralization of calcium carbonate in aqueous solutions starting from its initiation was studied by time-resolved small-angle neutron scattering (SANS). SANS revealed that homogeneous crystallization of CaCO₃ involves an initial formation of thin plate-shaped nuclei which subsequently reassemble to 3-dimensional particles, first of fractal and finally of compact structure. The presence of the egg-white protein ovalbumin leads to a different progression of mineralization through several stages; the first step represents amorphous CaCO₃, whereas the other phases are crystalline. The formation and dissolution of the amorphous phase is accompanied by Ca²⁺-mediated unfolding and cross-linking of about 50 protein monomers showing the characteristic scattering of linear chains with a large statistical segment length. The protein complexes act as nucleation centers for the amorphous phase because of their enrichment by Ca²⁺ ions. SANS revealed the sequential formation of CaCO₃ starting from the amorphous phase and the subsequent formation of the crystalline polymorphs vaterite and aragonite. This formation from less dense to more dense polymorphs follows the Ostwald–Volmer rule.

Introduction

Living organisms are capable of developing inorganic minerals and biocomposites with complex architectures to fulfill important biological functions, such as skeletal support or protection of soft tissues.[1–4] These hierarchically ordered and multifunctional composites with size ranges from the nano- to the centimeter scale exhibit, through a combination of inorganic toughness with organic elasticity, mechanical properties that make them outperform their purely inorganic counterparts and other synthetic materials.[5] The inorganic mineral phase of such materials is formed over an insoluble organic matrix or mold, and the mineral phase is intimately associated with organic macromolecules, such as proteins, glycoproteins, polysaccharides, or proteoglycans.[6] Many of these biomacromolecules are highly acidic in nature, that is, they have a p*I* < 4 (the pH at

which they have no charge) and have been postulated to control nucleation, growth, crystal size, and the shape of the mineral phases.[7–11]

The calcified layer of avian eggshells consists of ∼95% mineral and ∼5% organic phase.[12] The mineral phase is basically calcite, the most stable polymorph of calcium carbonate. The eggshell is formed during the passage of the egg through the oviduct, with the various layers of the eggshell assembled sequentially as the egg passes through the successive oviduct sectors. In the case of chicken eggshells, ∼5 g of CaCO₃ is deposited within 22 h in an acellular medium. The eggshell calcification process can be divided into three stages. (1) During the initial stage the first crystals are deposited on specific nucleation sites (the so-called mammillary knobs) on the surface of the outer eggshell membrane. (2) A rapid mineralization occurs during the growth phase of the shell where the compact

[†] Helmholtz Research Center.

[‡] Johannes Gutenberg University.

(1) Lowenstam, H. A. *Science* **1981**, *211*, 1126–1131.

(2) Addadi, L.; Weiner, S. *Angew. Chem., Int. Ed. Engl.* **1992**, *31*, 153–169.

(3) Mann, S. *Biomineralization*; Oxford University Press: Oxford, 2001.

(4) Bäuerlein, E. *Biomineralization*; Wiley-VCH: Weinheim, 2004.

(5) Levi-Kalisman, Y.; Falini, G.; Addadi, L.; Weiner, S. *J. Struct. Biol.* **2001**, *135*, 8–17.

(6) Heuer, A. H.; Fink, D. J.; Laraia, V. J.; Arias, J. L.; Calvert, P. D.; Kendall, K.; Messing, G. L.; Blackwell, J.; Riecke, P. C.; Thompson, D. H.; Wheeler, A. P.; Veis, A.; Caplan, A. I. *Science* **1992**, *255*, 1098–1105.

(7) Mann, S. In *Biomineralisation: Chemical and Biochemical Perspectives*; Mann, S., Webb, R., Williams, R. J. P., Eds.; VCH Publishers: New York, 1989; Vol. 35, p 62.

(8) Linde, A.; Lussi, A.; Crenshaw, M. A. *Calcif. Tissue Int.* **1989**, *44*, 286–295.

(9) Weiner, S.; Addadi, L. *Trends Biochem. Sci.* **1991**, *16*, 252–256.

(10) Endo, H.; Schwahn, D.; Cölfen, H. *J. Chem. Phys.* **2004**, *120*, 9410–9423.

(11) (a) Heiss, A.; Jahnen-Dechent, W.; Endo, H.; Schwahn, D. *Biointerphases* **2007**, *2*, 16–20. (b) Heiβ, A.; Schwahn, D. In *Handbook of Biomineralization: The Biology of Biominerals Structure Formation*; Bäuerlein, E., Behrens, P., Epple, M., Eds.; Wiley-VCH: Weinhein, 2007; Vol. 1, pp 415–433.

(12) (a) Arias, J. L.; Fink, D. J.; Xiao, S. Q.; Heuer, A. H.; Caplan, A. I. *Int. Rev. Cytol.* **1993**, *145*, 217–250. (b) Arias, J. L.; Neira-Carrillo, A.; Arias, J. I.; Escobar, C.; Bodero, M.; David, M.; Fernandez, M. S. *J. Mater. Chem.* **2004**, *14*, 2154–2160.

shell (palisade layer) is formed. (3) During the final phase there is an arrest of the shell calcification during the cuticle deposition. Supersaturation is a prerequisite for calcium carbonate precipitation. In the chicken uterine fluid, bicarbonate concentrations are close to 100 mM, and the ionic calcium concentration ranges from 5 to 10 mM, the concentration of ionic elements is 60- to 100-fold hypersaturated relative to the solubility product of calcite.

Numerous efforts have been undertaken to identify and characterize the matrix molecules present in the mammillary and palisade layers of the eggshell. Eggshell matrix proteins can be subdivided into three groups: (i) ubiquitous proteins that also occur in other tissues of the body, (ii) egg white proteins, and (iii) uterine proteins unique to the process of eggshell formation. *Osteopontin* is an ubiquitous phosphorylated glycoprotein, which is found at high concentration in bone and kidney, is also present in the eggshell.[13] It is localized in the core of the eggshell membrane fibers, at the bases of mammillae and in the outer palisade layer, but also throughout the palisade layer.[14] Eggshell osteopontin is likely to be a potent and phosphorylation-dependent inhibitor of calcium carbonate precipitation. During the eggshell formation, it may act as an inhibitor of calcite crystal growth or may modulate the rate of calcium carbonate precipitation from the supersaturated uterine fluid. *Ovalbumin* was the first egg white protein revealed in the shell matrix by N-terminal amino acid sequencing and immunochemistry.[15] Its presence in uterine fluid is predominant at the initial stage of eggshell formation,[16] and it is localized in the mammillae of the eggshell.[15] *Ovotransferrin* and *lysozyme* are also present in eggshell membranes at high levels and are also elevated in uterine fluid during the initial stage of shell formation; their intramineral localization is limited to the mammillary knobs.[17,18] Ovalbumin, lysozyme, and ovotransferrin are major proteins of the egg white, representing 54, 3.5 and 12% of egg white, respectively. Still, the role of these proteins in calcium carbonate mineralization is not well understood. They arrive via passive diffusion through the oviduct lumen. However, the uterus also synthesizes these proteins. Ovotransferrin and lysozyme modified the morphology of calcite crystals grown in vitro, suggesting some role in controlling calcium carbonate formation. As these three proteins are known for their antimicrobial properties they have been assumed to have a chemical protective function during avian embryonic development.[17,18] The *uterine proteins* involved in the process of eggshell formation comprise a number of shell proteins and proteoglycans that are only synthesized by tissues involved in eggshell calcification. Most of them have been identified only in the domestic hen. Their role in calcium carbonate mineralization is still unclear.

A number of observations support the idea that the eggshell matrix components regulate eggshell mineralization. (i) The composition of the uterine fluid changes at different stages of shell formation. Each phase of shell mineralization (nucleation, rapid crystal growth and the completion of shell formation) is associated with a specific distribution of biological macromolecules of the uterine fluid.[16] This may be related to a sequential alteration in gene expression and/or protein secretion by the uterus cells during eggshell formation.[16] (ii) The induction time for calcium carbonate precipitation is reduced by the uterine fluid during the formation of mammillary cores. This indicates that the distribution of macromolecules at the onset of calcification promotes crystal nucleation. In contrast, the total uterine fluid collected at the end of calcification inhibits the precipitation of calcite. This behavior has been observed for crystallization inhibitors that have a strong affinity for target crystal surfaces. At low concentrations, these inhibitors act as substrates promoting nucleation and favoring precipitation due to their stereochemical affinity to the crystal surface.[19] A possible explanation relies on the so-called ionotropic effect. A local maximum of the Ca^{2+} concentration in regions close to negatively charged regions of the protein might favor nucleation. In contrast, at higher concentrations the excess inhibitor binds to the crystal surfaces thereby blocking further growth. This inhibiting effect should be more pronounced for negatively charged (i.e., acidic) proteins.

The nature of the interaction between matrix molecules and the mineralization process is poorly understood. Protein adsorption is affected by the protein surface properties (electrical charge density, conformation and hydrophobicity) as well as solution conditions (pH, ionic strength, etc.). These parameters also affect the protein structure. In addition, electrostatic interactions play an important role, especially with hydrophilic surfaces such as calcite as shown by investigating the effect of model peptides of similar size and conformation, but with different charges (isoelectric points).[20] Therefore, at a given pH, their surface charges are different. These experimental results indicate that the dominant mechanisms accounting for adsorption are hydrophobic and electrostatic interactions. These peptides adsorb at different crystal faces in accordance with their net electrostatic attractions (or repulsions). These hypotheses are also supported by the importance of noncollagen proteins with carboxyl groups in bone calcification. In eggshell, highly sulfated proteoglycans are likely to influence mineralization by electrostatic interactions. Protein phosphorylation is another post-translational modification that has been shown to be crucial in other systems.[21,22]

In spite of intense research on the ultrastructure, composition, and presence of organic macromolecules in the eggshell matrix, our information concerning the molecular mechanism of eggshell mineralization is still limited. It is clear from all the above-reviewed results that the matrix components play an active role in the control of growth kinetics and of crystal morphology. We believe that the understanding of the role of the proteins and elementary processes involved in the eggshell formation will lead to a better understanding of the complex process of biomineralization. Calcium carbonate is an extremely widespread biomineral. The polymorphs calcite, vaterite, and aragonite are not only found in avian eggshells but also in shells

(13) Pines, M.; Knopov, V.; Bar, A. *Matrix Biol.* **1995**, *14*, 765–771.
(14) Fernandez, M. S.; Escobar, C.; Lavelin, I.; Pines, M.; Arias, J. L. *J. Struct. Biol.* **2003**, *143*, 171–180.
(15) Hincke, M. T. *Connect. Tissue Res.* **1995**, *31*, 227–233.
(16) Gautron, J.; Hincke, M. T.; Nys, Y. *Connect. Tissue Res.* **1997**, *36*, 195–210.
(17) Gautron, J.; Hincke, M. T.; Panhéleux, M.; Garcia-Ruiz, J. M.; Boldicke, T.; Nys, Y. *Connect. Tissue Res.* **2001**, *42*, 255–267.
(18) Hincke, M. T.; Gautron, J.; Panhéleux, M.; Garcia-Ruiz, J. M.; McKee, M. D.; Nys, Y. *Mater. Biol.* **2000**, *19*, 443–453.

(19) Weissbuch, I.; Lahav, M.; Leiserowitz, L. *Crystal Growth Design* **2003**, *3*, 125–150.
(20) Ajikumar, P. K.; Vivekanandan, S.; Lakshminarayanan, R.; Jois, S. D. S.; Kini, R. M.; Valiyaveettil, S. *Angew. Chem., Int. Ed.* **2005**, *44*, 5476–5479.
(21) Kröger, N.; Lorenz, S.; Brunner, E.; Sumper, M. *Science* **2002**, *298*, 584–586.
(22) Müller, W. E. G.;.; Boreiko, A.; Schloβmacher, U.; Wang, X.; Tahir, M. N.; Tremel, W.; Brandt, D.; Kandoorp,; J, A.; Schröder, H. C. *Biomaterials* **2007**, *28*, 4501–4511.

of mollusks and skeletons of echinoderms.[23] In addition, it was found from investigations on sea urchin larval spicules that in the early stages of spicule growth amorphous CaCO₃ is present as a transient precursor. The amorphous phase transforms by-and-by into calcite, the stable crystalline phase.[24–26] Another example for the transformation of amorphous calcium carbonate (ACC) into a crystalline phase was observed in larval shells of marine bivalves and the crustacea *Porcellio scaber*. It was shown that the mineral deposited in the initial steps of the biomineralization was amorphous and transformed subsequently, in part, into aragonite.[27] Similarly, a recent study reported a transient formation of ACC which subsequently transformed to a more stable crystalline phase during the formation of quail eggshells.[28] It is assumed that the transformation of ACC into a crystalline phase is much more widespread in biology than it is known to date, but because of its solubility and the difficulty of its detection might be often overlooked, especially when intimately associated with a crystalline phase.

In this contribution we present the results of time-resolved *in situ* studies starting with the early stages of crystallization of calcium carbonate in the absence and in the presence of the egg-white protein ovalbumin by means of small-angle neutron scattering (SANS). To the best of our knowledge, this paper represents the first detailed study of mineralization in the presence of protein using the technique of SANS. We will first present experimental data which will then be interpreted and discussed in context with underlying theoretical considerations in literature whereas the underlying laws of small angle neutron scattering are described in the Supporting Information.

Experimental Section

Sample Preparation and Characteristics. Ammonium carbonate (p.a.), sodium hydroxide (pellets, p.a.) and ovalbumin (>98% on dry substance) were purchased from Acros, while calcium chloride tetrahydrate (99.995%, suprapur) was purchased from Merck. D₂O was purchased from Chemotrade and had a purity of 99.8%. All experiments were performed using ultrapure water.

Neutron Scattering Experiments. The neutron experiments were performed using the KWS1 diffractometer at the FRJ-2 research reactor of the Helmholtz research center Jülich.[29] The experiments were performed with neutrons of wavelength of 7 Å with a 20% half-width of maximum and sample-to-detector distances from 20 to 2 m to overlap the whole possible Q interval. The data obtained from the samples were corrected for background scattering, sensitivity of the individual detector channels, and finally evaluated in absolute scale from calibration with a secondary standard. The scattering from pure solvents were measured and used for background correction. The transmission describing the decrease of nonscattered neutrons by the sample was automatically measured for all spectra.
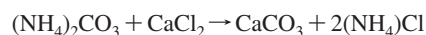
Light Scattering Experiments. Static (SLS) and dynamic (DLS) light-scattering measurements were performed with an ALV-SP86

goniometer, a Uniphase HeNe laser (25 mW output power at 514.50 nm wavelength), an ALV/High QE APD avalanche diode fiber optic detection system, and an ALV-5000 correlator. The static scattering intensities were analyzed according to mean square radius of gyration $R_g = \sqrt{<R^2>_z}$ (eq 3, Supporting Information), and the second virial coefficient A_2. The correlation functions from DLS showed a broad but monomodal decay and were fitted by a sum of two exponentials, from which the first cumulant Γ was calculated. The z average diffusion coefficient D_z was obtained by extrapolation of Γ/Q^2 to $Q = 0$ and to infinite dilution. The inverse z-average hydrodynamic radius $R_H = 1/<1/R>_z$, was evaluated by formal application of Stokes law. The solutions of 2 g/L ovalbumin containing varying salts were measured in water from 30 to 150° in steps of 10°. Prior to measurement, the solutions were filtered through 200 Å pore size Anotop filters (Millipore LG). Static light scattering intensities were accumulated using an incidence angle of 30°. The refractive index increment was measured by a home-built Michelson interferometer as described elsewhere.[30]

UV and CD Spectroscopy. UV−vis were recorded on a Hitachi U-3000 spectrophotometer in the range of 7000−2000 Å, CD spectra were recorded on a Jokim Yvon CD6 spectrophotometer in the 1800−3100 Å range. Photoluminescence spectroscopy was performed on a Bruins Omega-10 spectrometer with excitation wavelengths being in the range of 2500−2900 Å.

Transmission Electron Microscopy. Products were further characterized by transmission electron microscopy (TEM) on a Philips 420 instrument (acceleration voltage: 120 kV) and - for high resolution imaging and energy dispersive X-ray (EDX) analysis - a FEI Tecnai F30 ST (operated at an extraction voltage of 300 kV) equipped with an EDAX energy dispersive X-ray spectrometer, respectively. For the investigation of the samples using HRTEM (TECNAI F30 with FEG), the substance was suspended in methanol and afterward several drops of this suspension were placed on a copper grid with a holey carbon film.

Gas Diffusion Technique. The mineralization of CaCO₃ was performed using a gas diffusion technique by thermal decomposition of ammonium carbonate which involved the initiation by the diffusion of carbon dioxide and ammonia into a 0.1 M aqueous CaCl₂ solution according to the chemical reaction:

$$(NH_4)_2CO_3 + CaCl_2 \rightarrow CaCO_3 + 2(NH_4)Cl$$

The evolution of the pH was monitored using a pH electrode in a similar setup (Figure 10, *vide infra*). Mineralization was explored for concentrations of 0, 2.5, 5, and 7.5 mg ovalbumin per mL water. All experiments were performed at a temperature of 30 °C and pH of 10 which was chosen in order to maintain a sufficient concentration of carbonate ions during the whole mineralization process. The mineralization process was initiated and performed in a closed stainless steel container with two sapphire windows transparent for neutrons and a temperature control. The ammonium carbonate was filled in a separate beaker about 5 cm far from the sample container or "cell" which was placed in the neutron beam for in situ SANS experiments. The experiments were performed for about 12 h at two fixed detector-to-sample distances of 20 and 4 m. Samples were analyzed every 15 min for the first 4 h and then every 30 min.[31,32]

Scanning Electron Microscopy, Differential Thermal Analysis, and Measurement of pH and [Ca²⁺] Evolution. A slightly closed crystallization flask of 250 mL in volume was placed in a desiccator with a side tube, through which the cable of the pH and ion sensitive electrode was conducted outside to the processing unit. We used a WTW SenTix 81 pH electrode with automatic temperature compensation and a WTW pH 340 processing unit to monitor the pH value in intervals of 10 min for 2000 min. The crystallization

(23) Lakshminarayanan, R.; Jun Loh, X.; Gayathri, S.; Sindhu, S.; Banerjee, Y.; Kini, R. M.; Valiyaveettil, S. *Biomacromolecules* **2006**, *7*, 3202–3209.

(24) Levi, Y.; Albeck, S.; Brack, A.; Weiner, S.; Addadi, L. *Chem.−Eur. J.* **1998**, *4*, 389–396.

(25) Beniash, E.; Aizenberg, J.; Addadi, L.; Weiner, S. *Proc. R. Soc. London, Ser. B* **1997**, *264*, 461–465.

(26) Raz, S.; Hamilton, P. C.; Wilt, F. H.; Weiner, S.; Addadi, L. *Adv. Funct. Mater.* **2003**, *13*, 480–486.

(27) Weiss, I. M.; Tuross, N.; Addadi, L.; Weiner, S. *J. Exp. Zool.* **2002**, *293*, 478–491.

(28) Lakshminarayanan, R.; Jun Loh, X.; Gayathri, S.; Sindhu, S.; Banerjee, Y.; Kini, R. M.; Valiyaveettil, S. *Biomacromolecules* **2006**, *7*, 3202–3209.

(29) Neutron instruments at the FRJ-2 in Jülich, see: www.neutronscattering.de.

(30) Becker, A.; Köhler, W.; Müller, B. *Ber. Bunsenges.* **1995**, *89*, 600–605.

(31) Schwahn, D.; Balz, M.; Bartz, M.; Fomenko, A.; Tremel, W. *J. Appl. Crystallogr.* **2003**, *36*, 583–586.

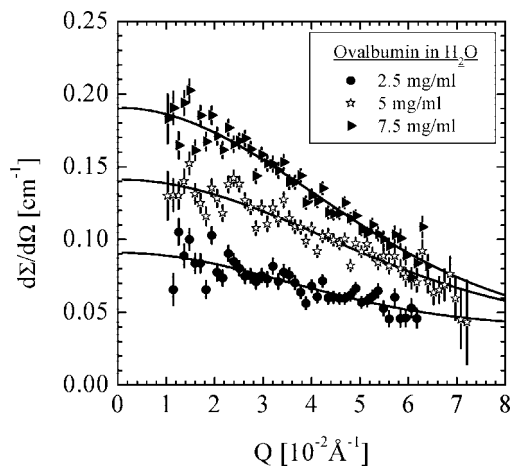(32) Schwahn, D.; Balz, M.; Tremel, W. *Phys. B* **2004**, *B350*, e947–e949.

Figure 1. Scattering from three concentrations of the protein ovalbumin in H_2O.

solution contained 1 mg/mL ovalbumin and 10 mM of $CaCl_2$. Samples for SEM respectively DTA were collected using glass slides at the bottom of the vessel. Prior to SEM analysis by means of a Zeiss DSM 940, the samples were sputtered with 100 Å of gold by a Baltec MED020. Differential thermal analysis (DTA) combined with thermal gravimetry (TG) was carried out on a Perkin-Elmer Pyris 6 TGA instrument.

Results

To set the stage for the mineralization of $CaCO_3$ in the presence of ovalbumin, we first studied the structure of native ovalbumin in aqueous solution as well as the effect of Ca^{2+} cations on the structure and solution behavior of the protein. To differentiate the homogeneous crystallization of $CaCO_3$ from processes mediated by the protein, we describe in the second section the results obtained for the homogeneous mineralization of $CaCO_3$. Finally we use our understanding obtained from the study of the individual components to describe the effect of ovalbumin on the mineralization of $CaCO_3$. As it turns out, this process is the sum of at least three individual subprocesses where ovalbumin first acts as a nucleation initiator and finally mediates the transformation from an amorphous phase to the crystalline polymorphs.

Study of Ovalbumin in Water. In an initial study we used SANS to characterize ovalbumin in aqueous solution. Figure 1 shows the scattering behavior for three concentrations. The data were fitted using Guinier's law (eqs 2 and 3 in the Supporting Information). From this fit two parameters, namely R_g and the extrapolated forward scattering $d\Sigma/d\Omega(0)$, were derived. An average R_g of (30 ± 0.5) Å and a linear dependence of $d\Sigma/d\Omega(0)$ from the ovalbumin concentration were found in agreement with eq 2 (in Supporting Information). The slope of $d\Sigma/d\Omega(0)$ gave a value of $V/(N_A d) \Delta\rho^2 = (20 \pm 0.7)$ mL^2/g, where N_A is the Avogadro number, d is the mass density and V is the molar volume of the protein (both values known, see Table 1 in Supporting Information). Thus, a coherent scattering length density $\rho = 1.64 \; 10^{10}$ cm^{-2} of ovalbumin in H_2O was determined.

In a subsequent study, we characterized ovalbumin (7.5 mg/mL) with variations in D_2O content and thereby the scattering contrast (Figure 20, Supporting Information, and Figure 2a,b). The relationship of $d\Sigma/d\Omega(Q)$ at $Q = 0$ is best described by a linear equation according to $\sqrt{d\Sigma/d\Omega(0)} = \sqrt{cV/(N_A d)} \; \Delta\rho$, where c is representative of the ovalbumin concentration in g/mL leading to a linear change with $\Delta\rho = (\rho_{Ovalbumin} - \rho_{Water})$. At

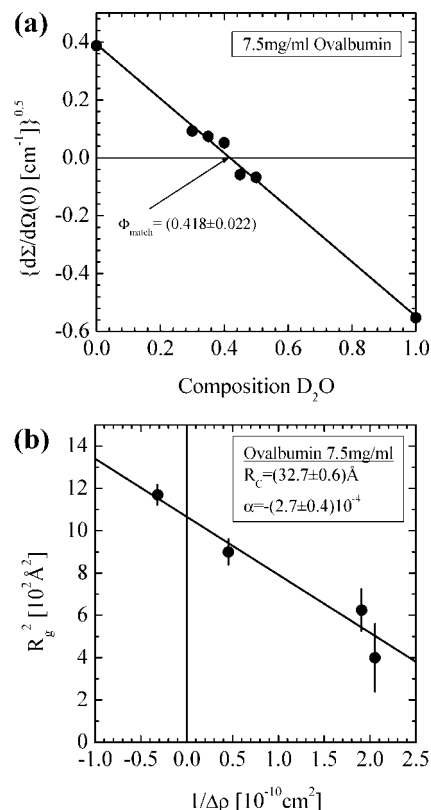**Figure 2.** (a) Matching condition of ovalbumin at 41.8 D_2O content. (b) Plot of R_g^2 versus $1/\Delta\rho$.

41.8% D_2O content the graph intercepts the zero line. This indicates a matching of the protein scattering with water, and the results are consistent with SANS experiments on other proteins.[33] The parameters in Table 1 (Supporting Information) together with ρ_{H2O} yield the scattering length density of ovalbumin versus D_2O content (Figure 20, Supporting Information). A change of the protein scattering length density with the D_2O content, which is caused by the H/D exchange at the outer surface of the protein, can be readily observed.[33]

Figure 2b shows a plot of R_g^2 versus $1/\Delta\rho$. R_g^2 shows a negative slope of $\alpha = (2.7 \pm 0.4)10^{-4}$ and $R_g = 32.7 \pm 0.6$ Å at the intercept of $1/\Delta\rho = 0$. Generally, a finite slope α represents an inhomogeneous mass distribution inside the protein whereas a negative α results from a larger scattering length density or a more concentrated mass in the center of the protein. In this study, the interpolated R_g at $1/\Delta\rho = 0$ means that the protein was measured at the limit of infinite scattering contrast and, therefore, with no sensitivity to the internal structure of the protein. This contrasts with previous studies, where a slight positive slope was observed.[33]

Calcium-Induced Refolding and Aggregation of Ovalbumin in the Presence of $CaCl_2$. Different concentrations of ovalbumin were freshly prepared in 0.1 M $CaCl_2$ aqueous solution and the influence of $CaCl_2$ on the protein was examined using SANS (Figures 3a, b). The measurements shown in Figure 3a were performed 13 h after preparation. Compared with the native protein in Figure 1, a significantly different scattering behavior was found: The scattering at $Q = 0$ increased by a factor of 41 (indicated by the dashed line), R_g increased to a value of nearly 600 Å, and a Q^{-2} and Q^{-1} power law at intermediate and large
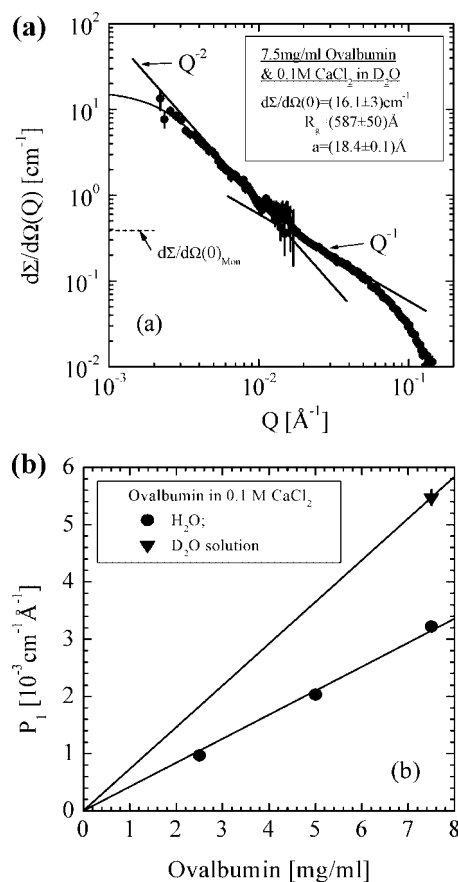
(33) Jacrot, B. *Rep. Prog. Phys.* **1976**, *39*, 911–953.

(a)

(a)

(b)

(b)

Figure 3. (a) Ovalbumin in 0.1 M CaCl$_2$ aqueous D$_2$O solution. An increase of dΣ/dΩ(0) is caused by cross-linking of about 50 proteins to an object with the conformation of a Gaussian linear chain as seen by the Q^{-2} and Q^{-1} power laws. The dashed line represents the scattering at $Q = 0$ of the corresponding ovalbumin monomer in Figure 1 after correction for scattering contrast. (b) Amplitude P_1 is proportional to the ovalbumin concentration.

Q were observed, respectively. This scattering can be interpreted in terms of a Gaussian linear chain scattering law with relatively large segments. For Gaussian chains a Q^{-2} power law is characteristic for Q larger than $1/R_g$, which changes to a Q^{-1} power law for Q values above the inverse size of the segment length.[34,35] dΣ/dΩ(0) from the 7.5 mg/mL ovalbumin H$_2$O solution had to be multiplied with 2.03 in order to correct for the contrast of ovalbumin in D$_2$O (Table 1). In this way, a dΣ/dΩ(0)= 0.38 cm^{-1} was achieved which is within 30% consistent with the calculated value of 0.3 cm^{-1} from the ovalbumin parameters in Table 1. The intensity at $Q = 0$ is determined (eq 2, Supporting Information) by the product of the protein volume fraction, the molar volume, and the scattering contrast according to $\Delta\rho^2$. This also means that the observed intensity increase can only be explained by an aggregation of about 50 proteins forming a linear chain. The Q^{-1} power law indicates rod-like segments which can be quantitatively analyzed (eq 5, Supporting Information).

In Figure 3b the amplitude P_1 is shown for different concentrations of the protein in D$_2$O and H$_2$O as derived from fits to $d\Sigma/d\Omega = P_1 Q^{-1}$ at large Q. For H$_2$O values these were strictly proportional to the protein concentration with $P_1 = 0$ at

$c = 0$ and a slope $\partial_C P_1 = \pi A_{\text{rod}} \Delta\rho^2/d = 0.42$ in units of cm^{-1}Å^{-1}/(g/mL) (d mass density of ovalbumin and eq 5, Supporting Information) was obtained. Thus, assuming $P_1 = 0$ at $c = 0$ a slope of 0.73 was determined for D$_2$O. Considering the two slopes obtained for the H$_2$O and D$_2$O solutions, a rod cross section of $A_{\text{rod}}=340$Å^2, i.e. the area occupied by the protein, is calculated when a value of 1.08×10^9cm^{-2} is added to the scattering length density of ovalbumin. This means that an increase of 6.6% in scattering length density of the protein consistently describes P_1 in Figure 3b. Such an increase in the protein scattering length density can be caused by about 130 Ca^{2+} ions distributed over 47 acidic (33 glutaminic acid and 14 aspartic acid) and 42 basic amino acids within the protein monomer as evaluated from the coherent scattering length b_c(Ca) $= 4.7\cdot10^{-13}$ cm of calcium and the relationship (0.066 V$_{\text{Prot}}$ ρ_{Prot})/ ($N_A b_c$(Ca))(for V_{Prot} and ρ_{Prot}, Table 1 in Supporting Information). This is about 20% of the total Ca^{2+} concentration for the highest ovalbumin concentration studied (7.5 mg/mL).

For Q values >0.05 Å^{-1}, the finite width of the protein rods could be determined from the scattering in D$_2$O (Figure 3a); the deviation from Q^{-1} is described by Guinier's law for rods according to $P_1 \propto \exp(-Q^2 a^2/4)$(eq 5, Supporting Information), which equates to the radius of slightly less than $a = 19$ Å. This radius translates to a rod area of 1130 Å^2 and, when compared with the area of 340 Å^2 from P_1, indicates that only 30% of that area is occupied by protein.

The above picture derived from SANS is supported by UV spectroscopic data and the results of dynamic light scattering experiments. The main absorption band in the UV spectrum of ovalbumin (attributed to the peptide bonds, phenylalanine and tyrosine chromophors) shows a bathochromic shift of 7 nm upon addition of CaCl$_2$, which can be attributed to an increase of β-sheets and/or less ordered segments at the expense of α-helix contributions.[36,37] Fluorescence measurements indicate that the reorganization of the protein monomer is completed within a few seconds. Comparative experiments on a 2 mg/mL solution of ovalbumin with 20 mM NaCl revealed monomodal behavior with a hydrodynamic radius $R_{\text{H}} = 28$ Å. Dynamic light scattering experiments of a 2 mg/mL ovalbumin solution containing 10 mM CaCl$_2$ allowed to monitor the slow increase of the hydrodynamic radius R_{H} with time. After about 5.5 h the system leaves the range of diffusively controlled motion. An exponential particle growth can be deduced from the exponential fit to the data in Figure 4 as shown by the solid line.

In summary, Ca^{2+} cations induce a refolding of ovalbumin and an exponential aggregation to rod-like chains (Figure 4a), which aggregate further to micrometer-sized fibers (Figure 4b).[38] Ovalbumin is known to undergo such refolding and aggregation processes induced by external thermal stress.[39–42] Detailed light scattering studies showed, that the heat-induced aggregation is reversible and follows also an exponential growth rate.[41] Based on the cumulant method, the ovalbumin fibers can be described as an intermediate between a flexible chain and a rigid rod,[39]

(34) Higgins, J. S.; Benoît, H. C. *Polymers and Neutron Scattering*; Clarendon Press: Oxford, 1994.

(35) Roe, R. J. *Methods of X-Ray and Neutron Scattering in Polymer Science*; University Press: Oxford, 2000.
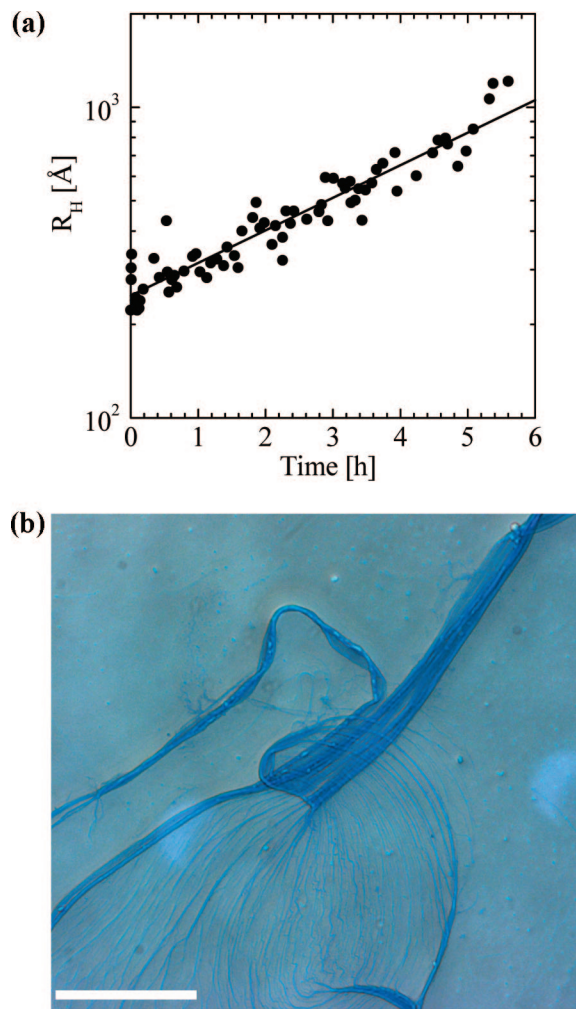
(36) Berman, H. M.; Westbrock, J.; Feng, Z.; Gillil, G.; Bhat, T. N.; Weissig, H.;.; Shindyalov, I. N.; Bourne, P. E. *Nucleic Acids Res.* **2000**, *28*, 235–242.

(37) The second derivative of the spectrum shows a shoulder in the trailing edge of the main maximum at 231 nm. Its position remains constant upon addition of the salt similar as a maximum at 280 nm (attributed to the tryptophane chromophor). A solution of ovalbumin without addition of salt reveals a shoulder at 195 nm (due to the peptide bonds), which has vanished after the CaCl$_2$ addition.

(38) Wolf, S. E. *Diploma thesis*, Johannes Gutenberg-Universität Mainz, 2005, Germany.

(a)

(b)

Figure 4. (a) Evolution of the hydrodynamic radius of ovalbumin upon addition of $CaCl_2$ (10 mM) obtained from dynamic light scattering experiments with time. (b) Protein fibers obtained by Ca-induced aggregation (staining with coomassie blue). Scale bar: 50 μm.

in consistence with the SANS data in Figure 3a. Hydrophobic-hydrophobic-interactions are responsible for this process,[39] the exposure of the β-sheet seems to be necessary to form an axial contact.[40] The mechanism is still under discussion: Nemoto et al. suggested an aggregation of dimers,[40] whereas Cryo-TEM studies of Weijers et al.[41,42] do not support this hypothesis.

Homogeneous Nucleation and Growth of Calcium Carbonate. The scattering patterns for a homogeneous crystallization of $CaCO_3$ in the absence of any protein additive are presented in Figures 5 and 6. The macroscopic cross-section versus scattering vector Q in Figure 5 shows characteristic stages of the nucleation and growth. Right after initiating the process of mineralization a weak scattering with a power law of Q^{-2} (measured exponent $\alpha = 1.95 \pm 0.2$) was observed, which then developed into a bimodal particle size distribution. At small Q, scattering from large compact particles with a Q^{-4} power law became visible

(39) Nemoto, N.; Koike, A.; Osaki, K.; Koseki, T.; Doi, E. *Biopolymers* **1993**, *33*, 551–559.
(40) Shirai, N.; Tani, F.; Higasa, T.; Yasumoto, K. *J. Biochem.* **1997**, *121*, 787–797.
(41) Pouzot, M.; Nicolai, T.; Visschers, R. W.; Weijers, M. *Food Hydrocolloid* **2005**, *19*, 231–238.
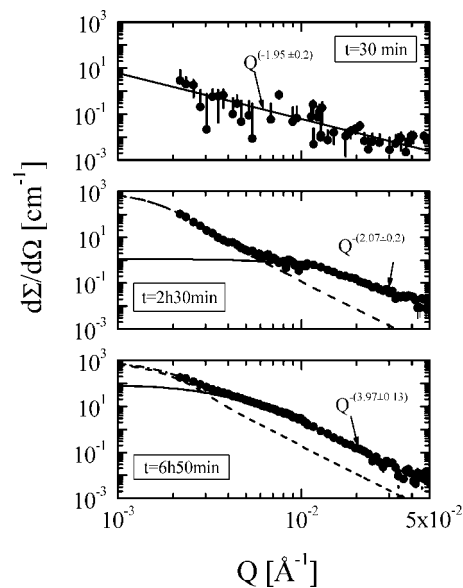(42) Weijers, M.; Visschers, R. W.; Nicola, T. *Macromolecules* **2002**, *35*, 4753–4762.

Figure 5. Scattering patterns observed during mineralization of $CaCO_3$ in 0.1 M $CaCl_2$ aqueous (H_2O) solvent without any further additives. A bimodal size distribution from very large and small minerals becomes visible as depicted as dashed and solid lines, respectively. The large and small ones represent heterogeneous and homogeneous nucleation and growth, respectively. The parameters from the small particles are summarized in Figure 6.
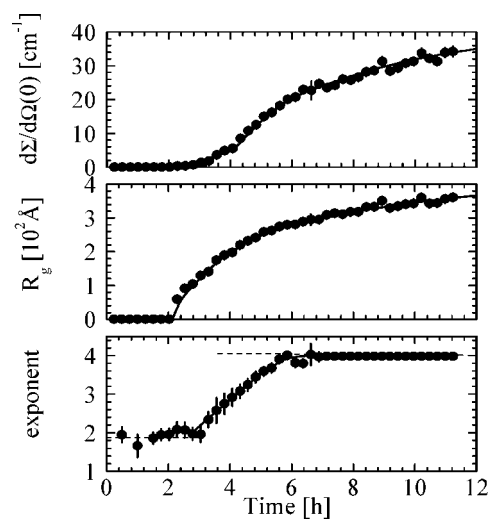

Figure 6. Parameters of scattering from Figure 5. (Bottom) Power law exponent from scattering at large Q, for example, from small particles. During the first 2.5 h plate shape (Q^{-2}) particles are observed and no area size could be determined. As depicted in (top) and (middle) $d\Sigma/d\Omega(0)$ and R_g, the small particles increases steadily for times later than 2 h. Between 3 and 6 h, a fractal dimensionality indicates a relatively open structure of the minerals.

(dashed line). The Porod constant "P_4" of these large particles is a measure of the surface area, which continuously increases with time (eq 6, Supporting Information). We attribute the formation of these particles to heterogeneous nucleation and growth which could occur at the surface of the container. In contrast, the formation of smaller particles (solid line) observed at larger Q can be attributed to homogeneous nucleation and growth.

Three parameters were derived from the large Q part, namely the extrapolated scattering at $Q = 0$, R_g, and the exponent of the scattering at large Q. The changes of these parameters
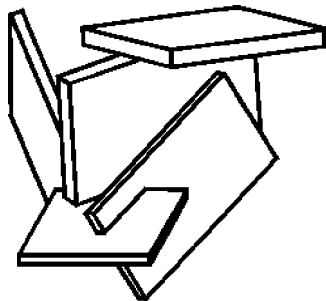
Figure 7. Model for the aggregation of plate shaped precursor mineral particles.
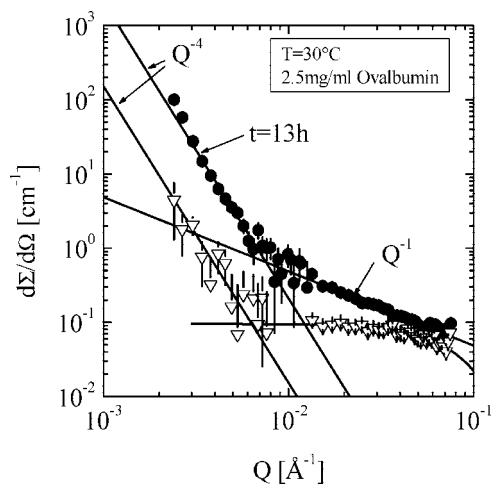

Figure 8. Scattering pattern before (▽) and after 13 h (●) of mineralization in the presence of ovalbumin. The scattering from the mineral and protein can clearly be distinguished.

with time are depicted in Figure 6. During the first 2–3 h of the mineralization reaction, the scattering was very weak. Only a slight increase in intensity was noticed due to the nucleation of small plate shape particles which best fit the data over the whole Q range for this time period. After two hours, particles with R_g of 60 Å were formed which continuously grew in size reaching 360 Å after 12 h. During this period, a complementary increase in $d\Sigma/d\Omega(0)$ was also observed. The exponent α of the power law at large Q was $\alpha \approx 2$ for the first three hours. It increased continuously for about three hours and reached a value of $\alpha \approx 4$ after about 6 h. According to Porod's Q^{-4} power law this indicates the formation of compact mineral particles. An exponent $\alpha < 4$ represents a mass fractal, for example, an open structure, whose compactness is proportional to the value of the exponent.[34] Figure 7 shows a cartoon of this process. The thin plates represent precursor particles of a three-dimensional particle with an open "house of cards" structure. This model is in contrast to the classical picture of nucleation and growth.

Mineralization of CaCO₃ in the Presence of Ovalbumin. In the presence of ovalbumin, a quite different mineralization process was observed. Figure 8 shows the scattering patterns before (▽) and 13 h (●) after initiation of the mineralization process. Scattering from large and small particles was observed. The scattering signal at large Q was mainly attributed to ovalbumin, whereas the signal at small Q is associated with the newly formed mineral phase. The protein was globularly shaped monomer before the start of the mineralization and had undergone a conformational change at the end of the mineralization process as shown by the Q^{-1} power law. This part of
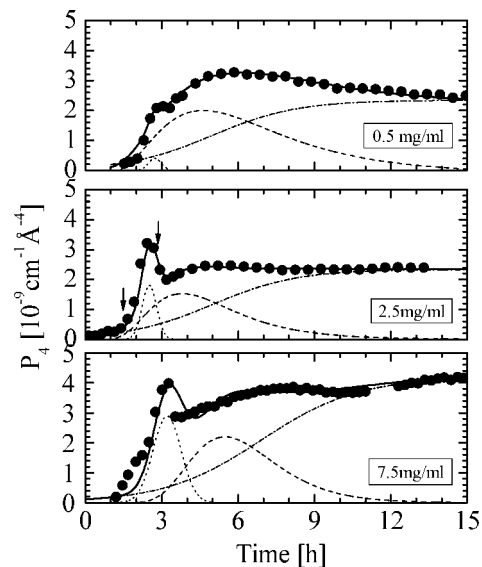

Figure 9. Progression of P_4 with time during mineralization in three 0.1 M CaCl₂ aqueous H₂O solutions (pH ≈ 10) different in ovalbumin concentration. The process was always started with freshly prepared samples. Three subprocesses become visible as indicated by the dashed lines.
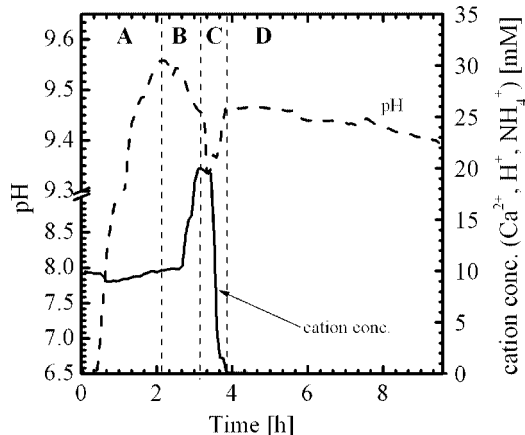

Figure 10. pH and Ca²⁺ concentration profile of the CaCO₃ crystallization in the presence of 1 mg/mL ovalbumin. (A) pH equilibrium is dominated by the uptake of NH₃. (B) pH equilibrium is dominated by uptake of CO₂. (C) CO₂ uptake and depletion of Ca²⁺ through the precipitation of CaCO₃ have similar order of magnitude, the Ca²⁺ supersaturation and the incipient CaCO₃ precipitation are reflected in the Ca²⁺ concentration profile. (D) pH value is dominated by the buffer effect of ovalbumin. (The apparent Ca²⁺ concentration in excess of the nominal Ca²⁺ content (10 mM) of the parent solution is due to the fact that the Ca²⁺-sensitive electrode is also sensitive to H⁺ and NH₄⁺).

scattering is discussed in more detail below in Figure 17. In contrast to the scattering pattern in Figure 3, no deviation from the Q^{-1} shape was observed here at large Q, indicating an apparently thinner rod like shape of the protein chains.

From the scattering at small Q, the size of the inorganic particles has to be at least in the micron range as only Porod's Q^{-4} power law was obeyed. Because the SANS instrument is limited for Q smaller than 10^{-3} Å⁻¹ particles larger than about 10^3 Å can not be determined completely. The sole information about these mineral particles is the Porod constant P_4, which is proportional to the total outer surface of a compact mineral particle (eq 6, Supporting Information). The evolution of P_4 during mineralization has been plotted in Figure 9 for samples with concentrations of ovalbumin of 0.5, 2.5, and 7.5 mg/mL. For each concentration, the evolution of the mineral surface is

illustrated by a characteristic graph pattern. Thus, after about 1.5 h, P_4 started to increase strongly, between 2.5 and 3 h a first pronounced peak was observed, after 6 to 8 h a broad and less pronounced peak became visible, which after about 12 h seemed to approach a stationary state. This process was influenced by the concentration of the protein. The first peak is comparatively small for the 0.5 mg/mL sample and more pronounced for the other two samples which possessed larger amounts of ovalbumin. In contrast, the second peak was slightly stronger for low protein concentrations. Thus, there appears to be an inverse relationship between the strength of first and second peak. In general, the time dependence of this surface area appears to have three contributions with distinct temporal signatures. The time constants are similar, but the amplitude of their contribution to the surface area is different, as the protein concentration is changed. The first process in particular always started after about 1.5 h and involved a strong increase in mineral surface area which after about 3 h passed through a maximum and sharply decreased afterward, suggesting a dissolution of this mineral phase or a reduction of surface due to a compaction, for example, a loss of inner and outer surface of this mineral phase (*vide infra*) . There also seems to be a strong correlation between the first process and the amount of protein. The second process is observed in the window between 3 and 12 h, whereas the third process remains the only one after 12 h. We describe these processes by Gaussian, log-normal, and tanh functions of t, respectively.

The progression of the Porod P_4 is paralleled by the pH profile of the mineralization process with time which displays a characteristic multistep behavior (Figure 10). After the start of the reaction, the pH of the solution rises within an induction period of approximately 2 h from 6.5 to 9.55. The pH change is due to the dissolution of ammonia (formed by the decomposition of $(NH_4)_2CO_3$) in water. The better solubility of NH_3 compared to that of CO_2 leads to the observed sudden pH change. This equilibrium adjusts within the next 30 min until the NH_3 vapor pressure in the gas phase matches the NH_3 partial pressure of the solution. Now CO_2 is absorbed by the solution over a period of about 30 min, during which the pH value passes through a minimum. This is the limit of equilibrium between the uptake of CO_2 by the solution and CO_2 depletion from the solution due to the precipitation of calcium carbonate. The subsequent growth and Ostwald ripening of the newly formed $CaCO_3$ nuclei after 4 h is not accompanied by a significant pH changes, and therefore the pH remains constant for the remaining duration of the experiment.

Assuming that after 12 h all Ca^{2+} ions in the solution have been precipitated into $CaCO_3$, we calculated a mineral volume fraction of 0.34% assuming the aragonite polymorph and from P_4 a radius of 5−6 μm for a spherical shape mineral for the 7.5 mg/mL ovalbumin solution. The two lower ovalbumin solutions in Figure 9 (0.5 and 2.5 mg/mL) show P_4 values 1.7 times smaller which means a correspondingly larger mineral size of about 10 μm. Thus the amount of protein seems to have a distinct effect on the final mineral size.

Identification of the Mineral by Contrast Variation. As demonstrated in Figure 9, the formation of large mineral particles in the μm range was observed in the presence of ovalbumin within a time interval between one and two hours after the start of the mineralization process. The corresponding scattering followed Porod's Q^{-4} power law with the amplitude P_4 measuring the total surface of the mineral (eq 6, Supporting Information). In addition we could monitor changes of the
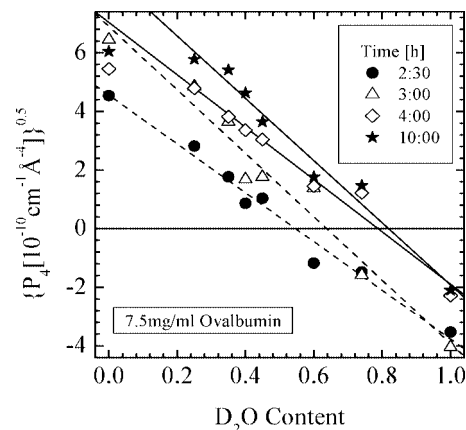

Figure 11. Square root of P_4 versus D_2O content for the given times. An identification of the amorphous polymorph could be made.

protein structure from the scattering at large Q. Both types of "particles" were visible separately because of their large difference in size. We also observed different stages during the process of mineralization. The aim of the following experiments was to acquire a better understanding of the sequences of mineralization shown in Figure 9 through additional SANS experiments by applying contrast variation using D_2O/H_2O mixtures.

The role of ovalbumin on the crystallization of calcium carbonate was monitored by measuring the process in the presence of 7.5 mg/mL ovalbumin in aqueous solutions with the different D_2O concentrations of $\Phi_{D_2O} =$ 0, 25, 35, 40, 45, 74, 82 and 100% and thereby with different scattering length densities of the solvent and contrasts as evaluated from the data in Tables 1 and 2, and as depicted in Figure 20 (Supporting Information). In Figure 11 the square root of P_4 is plotted versus D_2O content for the characteristic stages of mineralization. The results for each period of time could be described according to their proportionality with $\Delta\rho = |\rho_{Min.} - \rho_{Water}|$, assuming the same morphological structure of the mineral. At the intercept of $\sqrt{P_4} = 0$ the matching condition of the corresponding structure was achieved. After 2.5 and 3 h of mineralization when the first process was dominant we found a matching at (55 ± 5) and (64 ± 7)% D_2O content. This means, according to the matching condition of the amorphous $CaCO_3$ at 55% D_2O content (Table 2, Supporting Information), that after 2.5 h the amorphous phase is dominant. Thirty minutes later, a matching at (64 ± 7)% D_2O content was found, that is, only 50% of the amorphous phase was still present with vaterite as an additional polymorph. Only one hour later (total time = 4 h), when the amorphous mineral had dissolved, we found a matching at (79 ± 7)%, which subsequently increased slightly to (82 ± 7)%, indicating the formation of crystalline $CaCO_3$. The result points to the formation of the vaterite and aragonite polymorphs, respectively (Table 2, Supporting Information).

We could demonstrate the presence of amorphous $CaCO_3$ at this stage in solution by TEM-measurements as well (Figure 12). Samples taken 2.5 h after the start of the mineralization process were found to be amorphous. During the examination of these particles we observed the transformation from an amorphous to a crystalline phase within only few minutes. The transformation process seems to be induced by the high energy electron beam. Thus, the formation of primary amorphous particles after 1.5 h and their transformation to crystalline $CaCO_3$ could be verified independently by HRTEM.
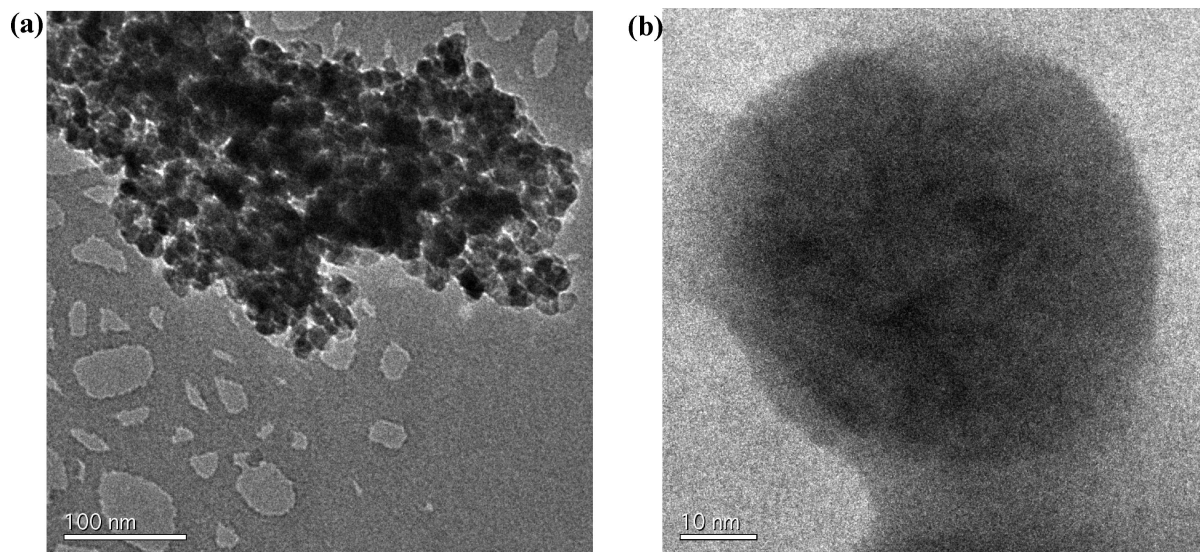
(a)

(b)

Figure 12. (a) TEM-graphs of samples collected from solution 2.5 h after the start of the mineralization process in the presence of ovalbumin demonstrating the presence of CaCO₃ nanoparticles with diameters ranging from 10−50 nm. (b) High-resolution TEM-graph (HRTEM) of one of the CaCO₃ particles shown in (a) demonstrating the presence of an amorphous particle.
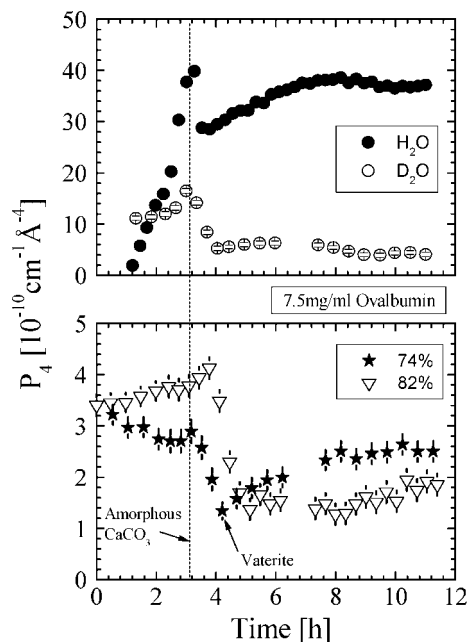

Figure 13. Porod amplitude versus time measured for different scattering contrasts. A peak from the amorphous polymorph became always visible after ∼3 h, after 4 h the minimum for the 74% D₂O solution identifies the vaterite polymorph whereas aragonite appears as the stable phase within 12 h.

The formation of the amorphous particles started after an induction period of about 1.5 h, reached a maximum volume fraction at about 2.5 h and was subsequently redissolved after 4 h and transforming to a crystalline polymorph. Figure 13 illustrates the formation sequence from the amorphous to the crystalline polymorphs during the mineralization by plotting P_4 versus time for solutions with D₂O concentrations of 0%, 74%, 82% and 100%. In all solutions the amorphous phase is visible as a peak in the window between 2 and 4 h. After this peak, a further increase of P_4 is observed for H₂O, whereas a slight decrease for D₂O. A pronounced minimum is found for the 74% D₂O solvent after 4 h, and after 5 h the 82% sample showed the smallest scattering. This behavior is understood when

considered with the coherent scattering length densities of the mineral polymorphs with respect to that of water as depicted in Figure 20 (Supporting Information). Thus, the increase of P_4 in the H₂O solvent occurs due to the formation of the mineral, as well as due to transitions of this mineral from the amorphous to the crystalline polymorphs, which cause an increase of the scattering contrast. In D₂O an overall decrease of P_4 is observed after 3 h of mineralization, i.e. there is a continuously decreasing scattering contrast according to $\Delta\rho = |\rho_{Min.} - \rho_{D_2O}|$, which overcompensates the increase of the scattering power due to the formation of the crystalline mineral phase. The 74% D₂O sample shows a pronounced minimum after 4 h of mineralization time which means that the vaterite polymorph (see Table 2, Supporting Information) is the dominating phase at this stage. The subsequent increase of P_4 is explained by a transition to the aragonite polymorph, where the matching conditions of aragonite in 84% D₂O aqueous solution is consistent with the lowest intensity observed in the 82% D₂O solution. The scattering length density of the CaCO₃ mineral in the presence of the ovalbumin continuously increased during the mineralization as can be derived from the positive and negative slopes of P_4 in the H₂O and D₂O solvents, respectively. These results provide the basis of an interpretation that CaCO₃ follows a polymorph sequence amorphous → vaterite → aragonite. Transformation to calcite as the most stable polymorph could not be observed in the time window of these experiments. Calcite formation may be excluded as its scattering contrast is close to that of vaterite, for example, the scattering from the 76% D₂O sample would show the lowest intensity (Table 2, Supporting Information).

Mineralization in Nearly Matched Condition for Protein and Amorphous CaCO₃. Another scattering experiment was conducted during the mineralization in 40% D₂O aqueous solution, representing the contrast conditions when scattering from the proteins and amorphous CaCO₃ nearly match and the crystalline calcium carbonate polymorphs are the main contributors to the scattering profile. A scattering pattern measured under such conditions after 7 h mineralization is shown in Figure 14. A bimodal size distribution of large and small particles is apparent. The Porod constant of the larger particles has already
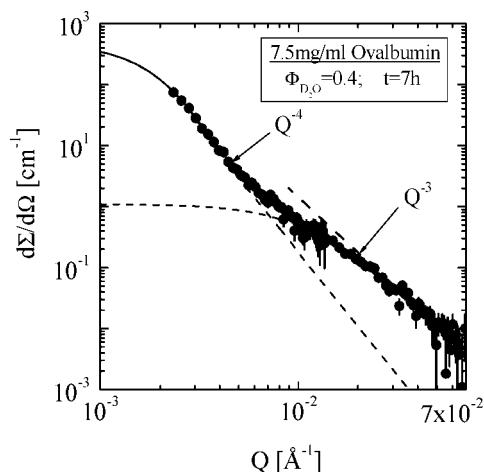
Figure 14. Scattering from mineralization in the 40% D_2O solution. In this solution, only the crystalline polymorphs are visible, for example, protein and ACC are matched. Besides large mineral particles small particles appear.
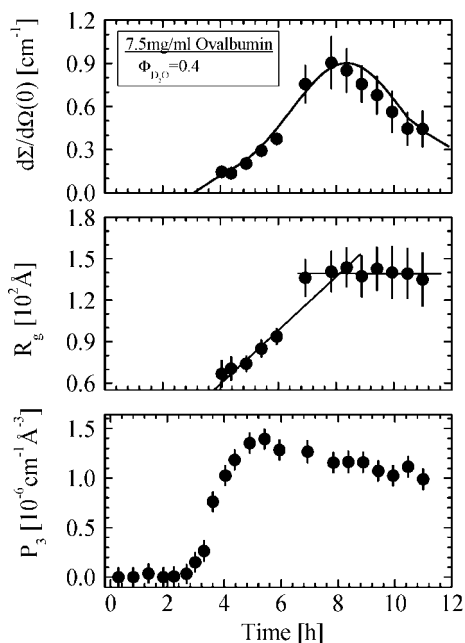

Figure 15. Parameters from small particle scattering in 40% D_2O solution.

been determined from Figure 11 whereas the fit parameters of the smaller particles, namely $d\Sigma/d\Omega(0)$, R_g, and P_3 are shown in Figure 15. These particles started to form about 4 h after initiating the mineralization, when only small quantities of the amorphous phase were present; their size increased from about 70 to 140 Å and remained constant for around 6 h, whereas the extrapolated scattering $d\Sigma/d\Omega(0)$ reached its largest value after around 8 h and then decreased again. This suggests that the number of these particles declined as R_g remained constant probably due to the agglomeration at the larger particles. The P_3 amplitude started to increase after 3 h, approached its maximum value after about 5 h and then slightly declined due to a decrease in the number of particles. The Q^{-3} power law indicates that this mineral had a porous structure whose origin could be water or protein inclusions as the scattering length densities of both are of similar values.[34] The identification of these particles is not so clear. They represent free particles of crystalline morphology superimposing incoherently (e.g., their
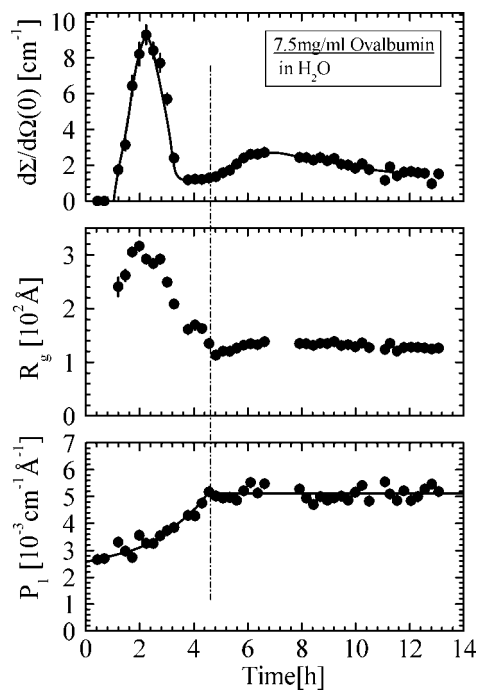

Figure 16. Parameters of mineral and protein during the mineralization in H_2O. (Bottom) P_1 amplitude becomes constant after 4 h. In the top and middle plots, two processes became visible. During the first 4 h a cross-linking and fragmentation of the protein simultaneously to the formation of the amorphous polymorph becomes apparent. Subsequently, a second process becomes visible (see Figure 13). The intensity ratios of both measurements indicate the formation of the aragonite polymorph.

intensity was added) to the scattering of the μm large minerals. By comparing the parameters of these particles with those measured within the same time interval using different scattering contrast and external conditions the following scenario could be drawn: (i) These particles were detected in H_2O showing increased maxima ($\cong 3\times$) (Figure 16). The scattering contrast of vaterite and aragonite give a factor of 5 and 3.9, respectively (Table 1 and 2, Supporting Information). Thus, it appears that these particles are most likely represented by an aragonite polymorph. (ii) The time period between 4 and 12 h is dominated by the "second" process of μm large particles representing vaterite as the dominating polymorph (Figures 9 and 12). (iii) The possibility of homogeneous nucleation and growth of $CaCO_3$ could be considered (Figures 6 and 7). Homogeneous formation of $CaCO_3$ in aqueous solution without any additives occurred within the same time interval but showed characteristic differences as the particle size was bigger by a factor two and it exhibited an open structure which underwent a continuous process of compaction (Figure 6). (iv) In summary, it appears more plausible that these small particles representing an aragonite polymorph result from the dissolution of the amorphous phase, thereby leading to a local supersaturation of ions for a new phase.

Evolution of the Protein Structure during Mineralization. The structural properties of the protein can be studied during the first 5 h of the mineralization because its scattering is well separated from that of the minerals (Figure 8). Similarly, the smaller mineral particles do not interfere, as they are formed at later stages of the mineralization process. The scattering patterns from a 2.5 mg/mL protein solution in H_2O (Figure 17) were monitored during the mineralization process shown in Figure 8 and 9. For the first 1.5 h the scattering of the protein is best described by Guinier's law indicating the compact structure of
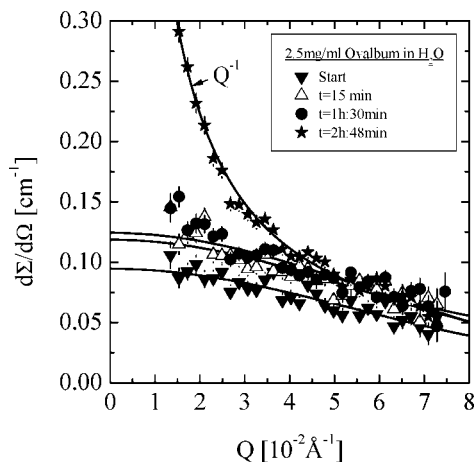
Figure 17. Time evolution of protein scattering during the mineralization. A gradual structural transition due to aggregation of the protein molecules is observed.

the native state. The slight increase of scattering after 90 min is the result of a 14.6% increase in the protein scattering length density which can be interpreted as a "loading" of the protein with about 280 Ca^{2+} ions. In a previous section (ovalbumin in the presence of $CaCl_2$) we estimated a loading of the protein by 130 Ca^{2+} ions from P_1 determined at large Q. After 90 min a gradual transition to a Q^{-1} power law is observed which was complete after nearly 3 h; a structural change of the protein was a continuous process during this time interval. The strong increase in intensity at low Q indicated that the process ("salting out") was accompanied by a cross-linking of protein molecules. From Figure 3 we determined a cross-linking of about 50 proteins in the presence of $CaCl_2$. The time interval of the "salting out" process as determined from Figure 17 is indicated by two arrows in Figure 9. In this time interval the formation of the amorphous polymorph (first process) proceeded and approached its maximum (indicated by the surface area or the Porod constant P_4). After the protein was "salted out", the amorphous phase started to dissolve or to densify as seen from the reduction of the amplitude P_4 in Figure 9.

Figure 16 shows the fit parameters from the scattering at large Q representing the mineralization in the presence of 7.5 mg/mL protein in H_2O. The amplitude P_1 continuously increased and approached a constant value after about 5 h. Within this time period a strong contribution from smaller particles, depicted as $d\Sigma/d\Omega(0)$, was found with the largest value of 9.3 cm^{-1} occurring slightly after 2 h of mineralization, and it is strongly reduced after 4 h. A second, but smaller and broader maximum is observed after 7 h. Parallel to the evolution of $d\Sigma/d\Omega(0)$ a plot of R_g vs time shows the same shape, a maximum length of about 300 Å at 2 h, which after about 4.5 h decreased to a constant value of about 130 Å. This observation further supports our interpretation of the directing effect of the protein in the mineralization of the amorphous phase. The first 4 h of mineralization were accompanied by strong structural changes of the protein conformation. The parameters $d\Sigma/d\Omega(0)$, R_g, and P_1 reflect the process of protein aggregation due to cross-linking through the mineral phase; $d\Sigma/d\Omega(0)$ and R_g acquire their largest values after 2 h, and they steeply decrease to a minimum after 4 h. A $d\Sigma/d\Omega(0)$ value of 0.19 cm^{-1} for the native ovalbumin monomer for a concentration of 2.5 mg/mL (Figure 1) indicates that protein complexes of about 50 protein monomers are formed after 2 h. This observation is consistent with the results illustrated in Figure 3, where a forward scattering of (16 ± 3)

cm^{-1} of the proteins in D_2O has to be divided by a factor of 2 in order to adjust for the contrast conditions of the protein in H_2O and D_2O. This time period is the same as that for the formation of the amorphous phase. After 4 h the protein complexes have dissolved, in parallel to the dissolution of the amorphous phase. A second but broader peak was observed after 4 h which may be due to the formation of a porous crystalline (possibly aragonite) polymorph, as depicted in Figure 15.

Discussion

The increase of CO_2 concentration in an aqueous 0.1 M $CaCl_2$ solution by thermal decomposition of ammonium carbonate and its diffusion into the solvent leads to $CaCO_3$ mineralization. The ovalbumin aggregates may be viewed as a complex of polypeptide chains in a conformation reminiscent of a linear Gaussian polymer chain with a relatively large statistical segment (Figure 3a). This protein structure represents an accumulation of Ca^{2+} ions which may act as nucleation center when the CO_2 concentration has passed a critical threshold value (according to the results in Figure 17 about 280 Ca^{2+} cations per monomer were accumulated after 1.5 h). The lateral extension of the enhanced Ca^{2+}-ion accumulation is determined by the size of the protein complex, which is on the order of 1000 Å as determined from R_g (Figure 3a). This might be the reason for the formation of μm sized minerals right from the beginning of the nucleation process. A similar process of complex formation was observed recently for polycarboxylate and Ca^{2+} using the technique of X-ray microscopy.[43]

A scenario representing this process of mineralization in the presence of ovalbumin is depicted in the sketch of Figure 18. After a critical "loading concentration" of Ca^{2+} cations has been reached, hydrogen bonds stabilizing the ovalbumin structure are broken. As a result, a partial unfolding and cross-linking of ovalbumin molecules in solution lead within a few seconds to a pronounced structural change, that is, an increase of nonordered β-sheet segments at the expense of the α-helix, as was deduced from UV, CD and fluorescence spectroscopy (Figure S-1, Supporting Information). An interesting aspect of this observation is that (i) an increase of the β-sheet fraction is triggered by the addition of Ca^{2+}, which, by virtue of a template effect, is considered to play a prominent role in the nucleation of $CaCO_3$.[44] (ii) The enhanced $CaCO_3$ nucleation associated with the Ca^{2+} triggered β-sheet formation points to a self-amplifying mechanism: the higher the Ca^{2+} concentration, the higher the $CaCO_3$ nucleating property of ovalbumin (Figure 18c). (iii) Ovalbumin exerts through multiple Ca^{2+} complexation a storage function, which might give a clue regarding the biological function of ovalbumin, which since its isolation more than hundred years ago is still unclear (Figure 18d,e).[45]

The replacement of Ca^{2+} by Mg^{2+} or the monovalent Na^+ leads to distinct changes in the UV and CD spectra. These spectral changes are compatible with a model, where protein refolding is induced only by calcium while magnesium and sodium exert only a minor effect at identical ionic strength of the solution.[38] Ovalbumin with an isoelectric point of 4.6 is a weakly acidic protein. We therefore assume that Ca^{2+} (which has a higher "complex binding constant" to carboxylate groups

(43) Rieger, J.; Thieme, J.; Schmidt, C. *Langmuir* **2000**, *16*, 8300–8305.
(44) (a) Mann, S. *Struct. Bonding (Berlin)* **1983**, *54*, 125–174. (b) Addadi, L.; Weiner, S. *Proc. Natl. Acad. Sci. U.S.A.* **1985**, *82*, 4110–4114.
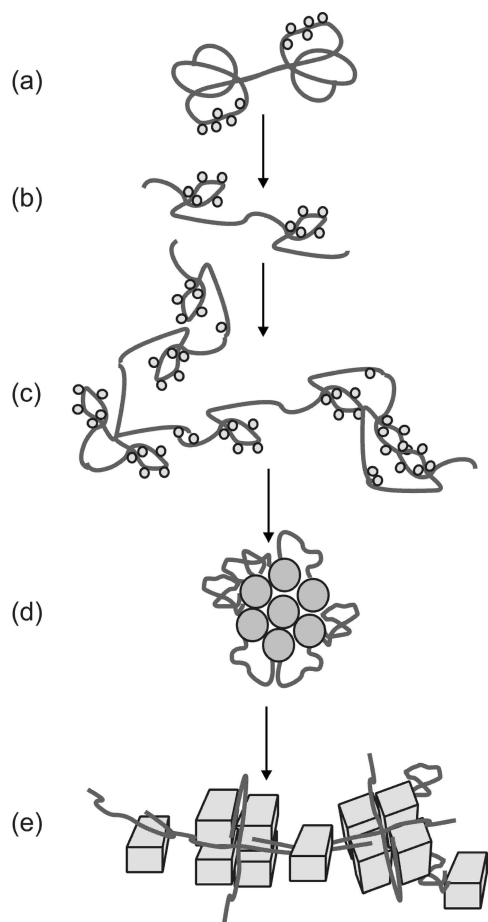(45) Huntington, J. A.; Stein, P. E. *J. Chromatogr. B* **2001**, *756*, 189–198.

Figure 18. Schematic representation of the CaCO₃ mineralization in the presence of ovalbumin (or polyelectrolytes in general). (a) At the onset, Ca^{2+} cations (small spheres) are bound to the protein by complexation through acidic side groups. (b) Ovalbumin rearranges immediately after cation binding. (c) Further cation binding triggers the break up of hydrogen bonds within the protein and eventually leads to a cross-linking of approximately 50 protein molecules. (d) The Ca^{2+} cations are the starting point for the subsequent formation of CaCO₃ nuclei (intermediate grey spheres) which are stabilized by surface bound ovalbumin (Figure 19, vide infra). Several of these nuclei can form a porous network of amorphous CaCO₃. (e) In the last step of the mineralization process, the preformed amorphous the CaCO₃ undergoes a series of phase transitions to the stable crystalline polymorphs (grey cubes). The protein remains attached to the crystallite surfaces.

than Na^+ or Mg^{2+46}) is coordinated to carboxylate groups at the periphery of the protein. Support for this model comes from a recent study where poly(acrylic acid) plays a comparable role as ovalbumin here by storing Ca^{2+} cations for mineralization as ACC particles.[47] Experimental evidence in this context is mainly based on the results of SANS and also of dynamic light scattering. The particle size of the minerals representing the three processes is of the order of at least micrometer and could not

(46) Kaim, w. Schwederski, B. *Bioanorganische Chemie*, Teubner,B. G. Stuttgart, 1991; Chapters 13−15.

(47) (a) Loges, N.; Graf, K.; Nasdala, L.; Tremel, W. *Langmuir* **2006**, *22*, 3073–3080. (b) Balz, M.; Therese, H. A.; Li, J.; Gutmann, J. S.; Kappl, M.; Nasdala, L.; Hofmeister, W.; Butt, H.-J.; Tremel, W. *Adv. Funct. Mater.* **2005**, *15*, 683–688. (c) Balz, M.; Therese, H. A.; Kappl, M.; Nasdala, L.; Hofmeister, W.; Butt, H.-J.; Tremel, W. *Langmuir* **2005**, *21*, 3981–3986. (d) The kinetics of a related system was investigated later by synchrotron X-ray reflectivity. DiMasi, E.; Kwak, S.-Y.; Amos, F. F.; Olszta, M. J.; Lush, D.; Gower, L. B. *Phys. Rev. Lett.* **2006**, *97*, 45503/1−4.

be determined with SANS. However, their total surface via Porod's constant P_4 could be evaluated and followed *in situ* as depicted in Figure 9 and 13. Its first maximum is associated with the formation of amorphous CaCO₃ particles as could be derived directly by contrast variation SANS experiments and electron microscopy. Another indication for the formation of CaCO₃ after about 3 h was given by the pH and [Ca^{2+}] evolution of the solution during the course of the crystallization (Figure 10). Both concentration profiles showed a characteristic multistep process. According to the Ostwald rule of stages, amorphous calcium carbonate (ACC) is formed in the presence of ovalbumin aggregated by a liquid−liquid phase separation (polymer/protein induced liquid precursor process, PILP).[48] The formation of amorphous calcium carbonate could be verified by TEM studies of samples taken after about 2.5 h from the solution (Figure 12). The sample contained small noncrystalline CaCO₃ particles with diameters of 300−400 Å that had agglomerated in solution. An analogous scenario was observed recently during the formation of CaCO₃ aggregates in the presence of polyaspartate and polyacrylate.[47]

The ACC is captured at the organic-solution interface in the form of particles which are stabilized by surface bonded ovalbumin (Figure 12). The final size of these particles after completion is in the micrometer range (Figure 19), which is consistent with the particle size estimated from SANS. The second increase in the pH value in Figure 10 is most probably caused by the incipient crystallization of the ACC particles. We also note the sudden increase of the Ca^{2+} concentration at the starting point of the nucleation process which may be caused by a release of Ca^{2+} cations bonded by the "ovalbumin cation buffer".

After 4 h, the particles representing the second and third process have crystallized. The second maximum of the progression was identified as vaterite, whereas the mineral particles of the final stage were identified as aragonite (Figure 11 and 13). The stable calcite phase could not be identified within the SANS experimental time frame of 12 h, but the identity of the calcite phase was confirmed after a reaction time of 2 d by SEM (Figure 19c). This observation is consistent with the kinetic picture of mineralization as discussed by Mann in ref 3.

Small porous probably aragonite particles with R_g of approximately 150 Å were formed after about 4 h after the initiation the mineralization process (Figure 15). This coincides with the time period when the amorphous phase was dissolving (Figure 9). Thus, there might be a relationship between these two processes. The amorphous phase might act as the reservoir of ions for the formation of aragonite whose porosity might be caused by water (hydrated phase) or protein inclusions present in the amorphous precursor phase. A corresponding crystallization scenario was given in a recent report by Weiner et al.,[49] who put forward the hypothesis that the disordered phase plays the same role in crystallization at organic−inorganic interfaces as the liquid phase in classical crystallization. We note that not only the ACC intermediate but also the final products of the crystallization still contain surface bound ovalbumin.[50] This interpretation is backed by the results of DTA measurements

(48) Gower, L. B.; Odom, D. J. *J. Cryst. Growth* **2000**, *210*, 719–734.

(49) Weiner, S.; Sagi, I.; Addadi, L. *Science* **2005**, *309*, 1027–1028.

(50) A thermogravimetric analysis of the CaCO₃/ovalbumin mineralization product showed an additional mass loss of 2.73% of compared to CaCO₃ precipitated in the absence of ovalbumin. Because ovalbumin shows a mass loss of 28.35% upon thermal decomposition, the ovalbumin content of the CaCO₃/ovalbumin composite should be approx. 9.6%.
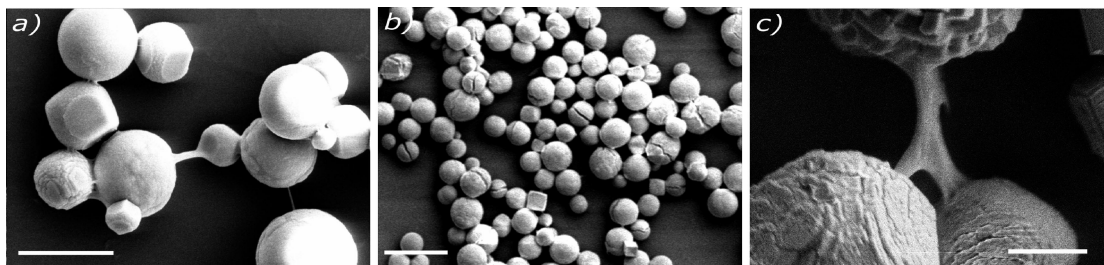
Figure 19. SEM images of CaCO₃ crystals obtained on glass slides by a gas diffusion reaction after a) 1,5 h b) 3 h and c) 2 days in a solution containing Ca²⁺ and 1 mg/mL ovalbumin. The images demonstrate the interconnection of the crystal by protein-fibers. The image (c) shows calcite mesocrystals with ovalbumin occluded between the crystal domains.[52] Scale bars: (a) 10 μm, (b) 20 μm, (c) 5 μm.

that are compatible with an organic portion of approximately 9.6 wt %. Most of the crystals isolated after the experiment were interconnected by proteinacous fibers, and they exhibit rough surfaces (Figure 19).

This indicates a change of a conventional ionic mechanism (homogeneous crystallization of calcium carbonate) to a protein mediated mechanism, an ovalbumin−Ca complex is the primary species in solution. Ovalbumin takes influence on the nucleation by complexation and capturing of Ca²⁺, thereby decreasing the free ion concentration and reducing the rate of ionic growth. It also favors the formation of rough and multiple crystals, whose surfaces are covered with chemisorbed protein. The protein acts by virtue of its acidic groups as a multifunctional ligand and it sticks to the crystallite surfaces in barnacle-like fashion (Figure 19). The existence of amorphous calcium carbonate nanoparticles in the size range of approximately 300−500 Å (from TEM) at the early crystallization stages show the hybrid product assembly from amorphous primary particles to amorphous aggregates with subsequent crystallization. ACC and vaterite (the kinetically stabilized polymorph) are known to form in the presence of aspartate and polyaspartate,[51] which is consistent with the formation of ACC and vaterite intermediates in the present case.

The mineralization of CaCO₃ in the presence of the ovalbumin has to be compared with homogeneous nucleation of CaCO₃ as determined in Figures 6 and 7. During the first 2−3 h, thin mineral plates of less than 30 Å thickness were formed which subsequently aggregated to particles of increasing size, first as fractal objects, and after 6 h as compact particles (Figure 6 and 7). This CaCO₃ formation is different from the classical picture of homogeneous nucleation and growth and obviously follows a pathway via the formation of intermediate mesocrystals (Figure 7) as proposed by Cölfen and Mann[52] and confirmed in several experiments.[53,54]

Summary and Conclusions

In this work, we have presented the results of time-resolved investigations of the crystallization of calcium carbonate using the technique of small-angle neutron scattering (SANS). We have followed the mineralization in situ from its early initiation using a gas diffusion technique. The mineralization process was studied both in the absence and presence of the egg-white protein ovalbumin. It was found that: (i) the crystallization process without ovalbumin starts immediately and yields crystallites in the size range of several μm, probably due to heterogeneous nucleation at

the glass surface of the cuvette. In addition, the formation of small particles was observed which may be attributed to homogeneous nucleation. This process showed three stages that involved thin CaCO₃ plates with a thickness of less than 30 Å as nuclei prior to their assembly to 3-dimensional particles with sizes between 50 and 350 Å in a mass-fractal structure with continuously increasing compactness. (ii) In the presence of the hen-egg protein ovalbumin amorphous calcium carbonate particles with sizes of several μm are formed within minutes after initiation. The subsequent mineralization proceeds through different polymorph structures. In the first process, an amorphous calcium carbonate phase was formed. This process runs parallel to an unfolding and cross-linking of the protein, which separates into smaller units when the amorphous phase redissolves (or undergoes a surface mediated compaction). During the formation and dissolution of the amorphous phase, two crystalline polymorphs were formed, first vaterite and after 12 h aragonite. (iii) A transition to the most stable polymorph calcite was not observed, but would be clearly visible as calcite has a similar scattering contrast as vaterite (Table 2, Supporting Information). The identification of the various polymorph phases was possible by using contrast variation techniques, a straightforward technique in neutron scattering, by performing the mineralization in D₂O/H₂O aqueous solutions of varying composition.

These in situ studies give a first clue concerning the role of ovalbumin in the eggshell formation by providing insight into the elementary steps of protein mediated CaCO₃ mineralization which is of importance for a better understanding of the nucleation and growth processes of minerals in biological systems. (i) Ovalbumin first acts as a "cation sponge" which locally increases the Ca²⁺ concentration. (ii) These Ca-rich pockets of ovalbumin aggregates seem to build nucleation centers for the incipient calcium carbonate formation. (iii) Calcium carbonate nanocrystals are stabilized by surface bound ovalbumin which is (iv) eventually occluded between the individual CaCO₃ crystallites, thereby forming a mesocrystal, i.e. an inorganic−organic hybrid material. In contrast, homogeneous calcium carbonate crystallization, for example, without any biological structures present, is determined by the formation of thin platelets as precursor particles.

(51) Manoli, F.; Dalas, E. *J. Cryst. Growth* **2001**, *222*, 293–297.
(52) Cölfen, H.; Mann, S. *Angew. Chem., Int. Ed. Engl.* **2003**, *42*, 2350–2365.
(53) Schwahn, Dietmar.; Ma, Yurong.; Cölfen; Helmut, *J. Phys. Chem.* **2007**, *111*, 3224–3227.
(54) Rieger, J.; Frechen, T.; Cox, G.; Heckmann, W.; Schmidt, C.; Thieme, J. *Faraday Discuss.* **2007**, *136*, 265–277.

Supporting Information Available: Essential details concerning the theoretical background of small angle neutron scattering and the contrast variation technique. This material is available free of charge via the Internet at http://pubs.acs.org.

JA801798H